Chinese Chemical Letters 35 (2024) 110050

Contents lists available at ScienceDirect

Chinese Chemical Letters

journal homepage: www.elsevier.com/locate/cclet

Benzo[4,5]imidazo[1,2-*a*]pyrimidine-based structure-inherent targeting fluorescent sensor for imaging lysosomal viscosity and diagnosis of lysosomal storage disorders

Jiao Chen[a,b,1], Zihan Zhang[a,1], Guojin Sun[a], Yudi Cheng[a,b], Aihua Wu[a], Zefan Wang[a,b], Wenwen Jiang[a], Fulin Chen[b,*], Xiuying Xie[a,c], Jianli Li[a,*]

[a] *Key Laboratory of Synthetic and Natural Functional Molecule of the Ministry of Education, Xi'an Key Laboratory of Functional Supramolecular Structure and Materials, College of Chemistry & Materials Science, Northwest University, Xi'an 710127, China*
[b] *Key Laboratory of Resource Biology and Biotechnology in Western China, Ministry of Education, Biomedicine Key Laboratory of Shaanxi Province, Lab of Tissue Engineering, the College of Life Sciences, Faculty of Life Science & Medicine, Northwest University, Xi'an 710069, China*
[c] *The Second Affiliated Hospital of Xi'an Jiaotong University, Xi'an 710004, China*

ARTICLE INFO

Article history:
Received 16 May 2024
Revised 22 May 2024
Accepted 24 May 2024
Available online 28 May 2024

Keywords:
Fluorescent sensor
Benzo[4,5]imidazo[1,2-*a*]pyrimidine
Lysosome
Viscosity
Lysosomal storage disorders
Structure-inherent targeting
Fluorescence imaging

ABSTRACT

Benzo[4,5]imidazo[1,2-*a*]pyrimidine-based derivatives play crucial roles in medicines, pesticides, tracers and photoelectric materials. However, their synthesis approach still needs to be optimized, and their fluorescent properties in intracellular microenvironment are unclear. Here, a Cu(II)-catalyzed cascade coupling cyclization reaction was successfully developed to synthesize benzo[4,5]imidazo[1,2-*a*]pyrimidine scaffold with mild reaction conditions, broad substrate scopes and high yields. After a system study, we found that compound **4aa** displayed an optimal viscosity-specific response with remarkable fluorescence enhancement (102-fold) for glycerol at 490 nm. Particularly, **4aa** possessed excellent structure-inherent targeting (SIT) capability for lysosome ($P = 0.95$) with high pH stability and large Stokes shift. Importantly, **4aa** was validated for its effectiveness in diagnosing lysosomal storage disorders (LSD) in living cells. The **4aa** also showed its potential to map the micro-viscosity and its metabolism process in zebrafish. This work not only affords an efficient protocol to fabricate benzo[4,5]imidazo[1,2-*a*]pyrimidine derivatives, reveals this skeleton has excellent SIT features for lysosome, but also manifests that **4aa** can serve as a practical tool to monitor lysosomal viscosity and diagnose LSD.

Lysosomes, the membrane-bound organelles and the primary degradative compartments of eukaryotic cells with a pH range of 4.5–5.5, have crucial functions of catabolizing and recycling cellular waste, cellular signal transduction, energy metabolism, and maintaining cellular homeostasis [1,2]. Viscosity as a crucial microenvironmental parameter of subcellular contributes to biological functions by affecting the mobility of substances [3,4]. It is reported that lysosomal viscosity ranges from 50 cp to 90 cp, while the accumulation of biomacromolecules in lysosomal storage disorders (LSD) leads to a significant elevation of lysosomal viscosity (Fig. 1a) [5-7]. In addition, the abnormal variation of viscosity is also associated with various diseases such as cancer, diabetes, neurodegenerative disorder, non-alcoholic fatty liver disease, *etc.* [8-15]. Therefore, precisely monitoring of lysosomal viscosity is of vital importance for evaluating lysosomal status and diagnosing lysosomal dysfunction-related diseases.

Fluorescent sensor is a popular and practical tool to detect various indicators in the subcellular microenvironment thereby achieving disease diagnosis. Due to the merits of non-invasive, spatial and temporal imaging, fluorescent sensors are very suitable to measure viscosity in biological systems [16-20]. To accurately monitor lysosomal viscosity, the priority is constructing a lysosome-targeted fluorophore. The common strategy is incorporating weakly alkaline units (*N*,*N*-dimethylethane-1,2-diamine or morpholine group) to fluorophore (Fig. 1b) since these acidotropic units facilitate to guide the fluorophore selective accumulation in acidic lysosome. Based on the mentioned strategy, many novel lysosome-targeted fluorophores have been reported, whereas the pH-sensitivity of them would interfere fluorescence signals when detecting lysosomal viscosity. To surmount this obstacle, the structure-inherent targeting (SIT) fluorescent sensor equipped with high pH-stability is highly desired for lysosomal viscosity.

* Corresponding authors.
E-mail addresses: chenfl@nwu.edu.cn (F. Chen), lijianli@nwu.edu.cn (J. Li).
[1] These authors contributed equally to this work.

https://doi.org/10.1016/j.cclet.2024.110050
1001-8417/

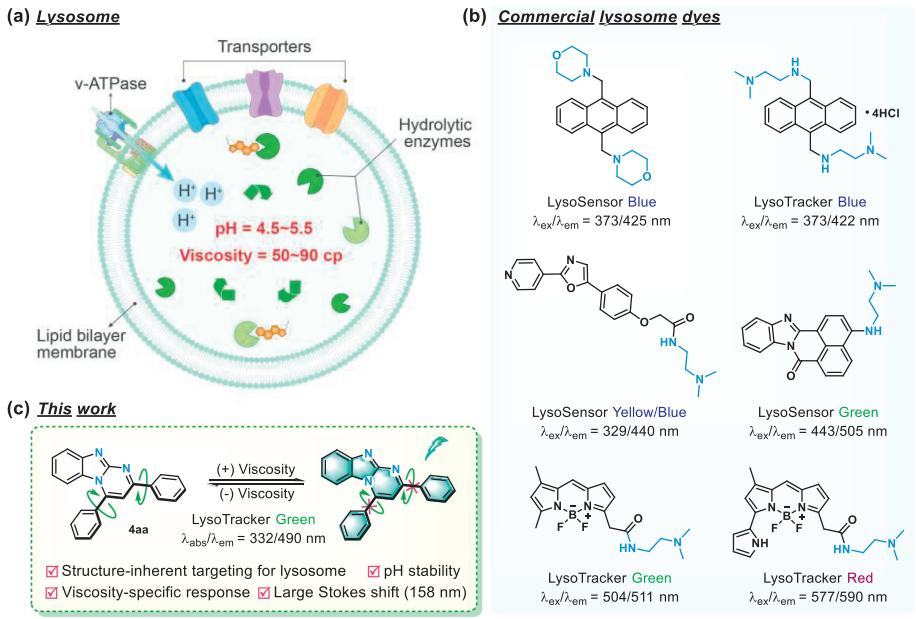

Fig. 1. (a) Schematic structure of lysosome. (b) Chemical structure of commercial LysoTrackers/Sensors. (c) The developed benzo[4,5]imidazo[1,2-*a*]pyrimidine-based structure-inherent targeting fluorescent sensor in this work.

Benzo[4,5]imidazo[1,2-*a*]pyrimidines, as one of the important nitrogen-containing fused heterocyclic compounds, exhibits exceptional photophysical properties and diverse biological effects [21-24]. It is noteworthy that this kind of multiple nitrogen-fused heterocycle skeleton has alkalescency, and its alkalinity is weaker than that of *N*,*N*-dimethylethane-1,2-diamine and morpholine units, exhibiting a certain capability to receive protons. Moreover, a moderate conjugate-plane structure of multiple nitrogen-fused heterocycle skeleton permits good ultraviolet absorbance and fluorescence emission. Thus, we envision that multiple nitrogen-fused heterocycle compound would serve as an acidotropic candidate for lysosome targeting imaging with improved pH stability. Consequently, an efficient method to construct this skeleton is important in current investigations. Among a range of options, the transition-metal-catalyzed multicomponent reactions (MCRs) in one pot, as a favorable and attractive synthetic strategy, have been validated in constructing benzo[4,5]imidazo[1,2-*a*]pyrimidine. For instance, 2-aminopyrimidine, aldehyde and alkyne/α,β-unsaturated ketone or their equivalents were utilized to achieve the synthesis of benzo[4,5]imidazo[1,2-*a*]pyrimidine skeleton *via* MCRs [25-27]. Recently, an iron-catalyzed [3 + 2 + 1] annulation strategy also has been developed to synthesize this scaffold from 2-aminobenzimidazoles and aromatic alkynes or acetophenone by using *N*,*N*-disubstituted amines as a one-carbon synthon [28,29]. Although powerful, some deficiencies such as the limited substrate scopes and expensive raw materials still restrict their further broad applications. Accordingly, exploring a more practical approach to establishing benzo[4,5]imidazo[1,2-*a*]pyrimidine skeleton is necessary.

The above considerations encouraged us to develop nitrogen-containing fused heterocycle-based fluorescent sensors for lysosomal viscosity. In this work, we disclose a novel and efficient Cu(II)-catalyzed coupling-cyclization that enables synthesizing benzo[4,5]imidazo[1,2-*a*]pyrimidine derivatives in high yields *via* three-component reaction of 2-aminobenzimidazole, versatile aldehydes and β-nitroalkenes, which is the first example that using nitroolefin as synthon to construct benzo[4,5]imidazo[1,2-*a*]pyrimidine scaffold. This reaction tolerates aryl rings/heterocyclic aromatic aldehydes and different nitroolefins with both electron-donating and -withdrawing groups, by which 53 compounds have been expanded successfully. Moreover, after a system investigation of optical properties, compound **4aa** not only displayed viscosity-specific fluorescence response with high pH stability as expected and large Stokes shift but also exhibited excellent structure-inherent targeting for lysosome (Fig. 1c), affording great potential in monitoring lysosomal viscosity and diagnosing LSD.

To fabricate benzo[4,5]imidazo[1,2-*a*]pyrimidine scaffold, initially, the combination of 2-aminobenzimidazole **1**, benzaldehyde **2a**, and β-nitrostyrene **3a** was tested as a model reaction. After a comprehensive optimization of reaction parameters, including copper catalysts, bases, reaction temperatures, and solvents (Table S1 in Supporting information), we identified the optimal conditions as follows: the reaction of **1** (1.2 equiv.), **2a** (1.0 equiv.) and **3a** (1.0 equiv.) in the presence of $Cu(OAc)_2$ (20 mol%), Cs_2CO_3 (2.0 equiv.) in *N*,*N*-dimethylformamide (DMF) at 110 °C for 10 h under the oxygen (O_2) atmosphere afforded **4aa** in 83% yield. The structure of compound **4aa** was verified through X-ray crystallographic analysis (CCDC: 1820030). Given the potential effects of different substituents on fluorescence properties, under the established optimal reaction conditions, we examined the generality of the substrate scope, such as electron-donating/withdrawing groups, aliphatic/aromatic (heterocyclic) groups, and halogen atoms. As shown in Fig. 2, the conversions of various aromatic aldehyde compounds (**4aa**–**4na**) were achieved. Meanwhile, the heteroaryl aldehydes of furan and thiophene proceeded smoothly, providing **4la** and **4ma** in 67% and 69% yields, respectively. A broad range of β-nitroalkenes with different substituents were well-tolerated to obtain the corresponding products **4ab**–**4an** in good to excellent yields. Notably, β-nitroalkene containing nitro and cyclohexyl groups provided **4ag** and **4an** in moderate yields. Furthermore, various aryl rings, heterocyclic aromatic aldehydes, and β-nitroalkenes were also successfully transformed to the corresponding products (**4a**–**4z**) in good to moderate yields. The results reveal high functional-group compatibility of this reaction with comparable yields.

The reaction mechanism was investigated according to a series of control experiments (Scheme S3 in Supporting information), which lent support that compound **1** first reacted with aldehyde **2a** to produce Schiff-base **A**, followed by coordinating with Cu(II) catalyst to form a copper complex **B**. Then **B** was deprotonated by

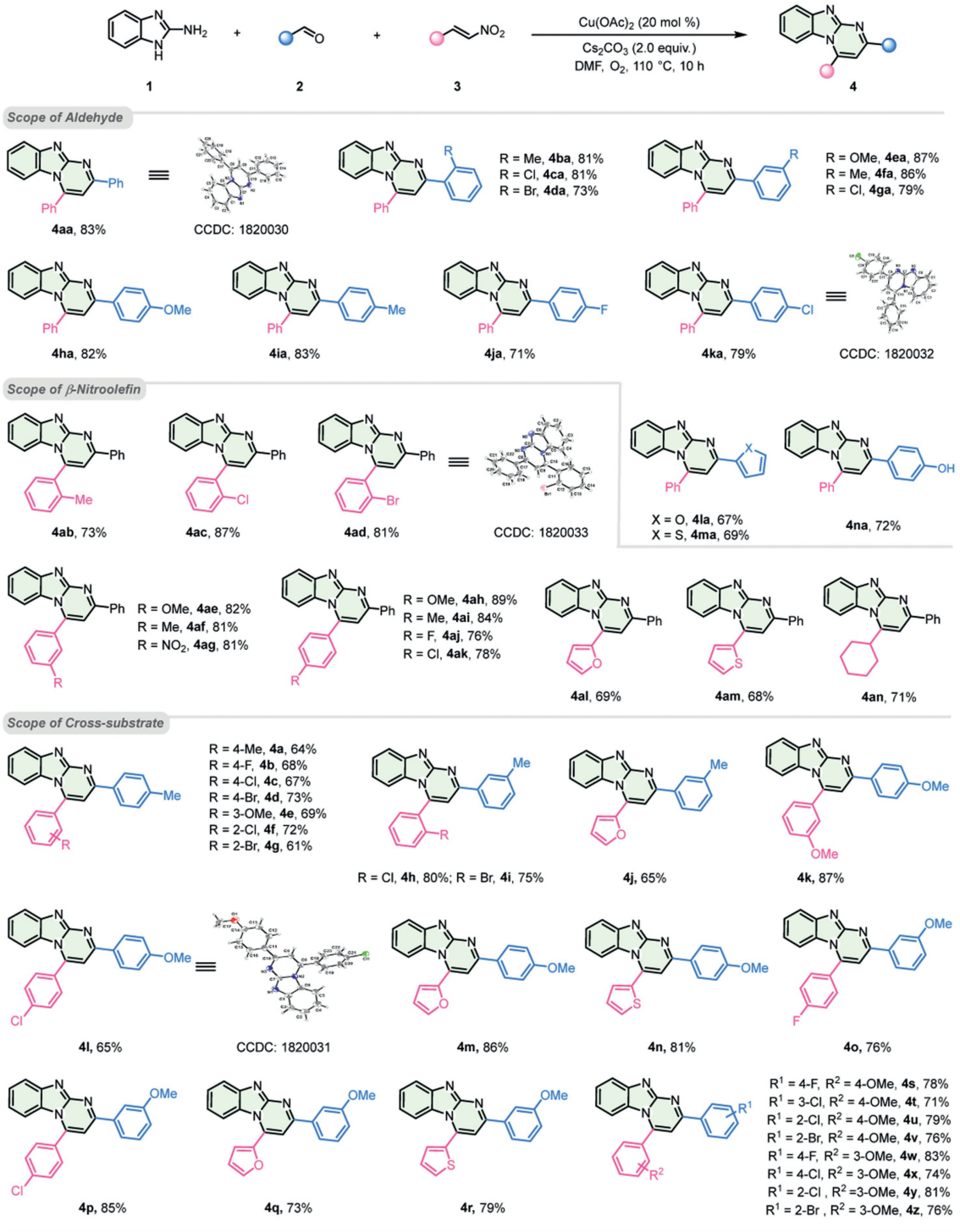

Fig. 2. Substrate scope for aldehydes and β-nitroalkenes. Conditions: **1** (1.2 mmol), **2** (1.0 mmol), **3** (1.0 mmol), $Cu(OAc)_2$ (20 mol%), Cs_2CO_3 (2.0 equiv.), DMF (6 mL), O_2 balloon, 110 °C; isolated yields.

Cs_2CO_3, providing intermediate **D** *via* an addition-cyclization with **3a**. The intermediate **D** was identified by high-resolution mass (Fig. S1 in Supporting information), and it was tautomerized to **E** and underwent elimination of HNO_2 as well as oxidation to give aim product **4aa** (Scheme S4 in Supporting information).

With various benzo[4,5]imidazo[1,2-*a*]pyrimidine derivatives in hand, their structure-properties relationships were investigated first. We selected 15 compounds with different electron-donating or withdrawing substituents at different positions to test their optical properties on absorbance/emission wavelength, molar extinction coefficient, lifetime, and absolute fluorescence quantum yield (Table S2 and Figs. S2–S5 in Supporting information). It manifests that these compounds have two absorption bands at ~340 nm and ~390 nm in organic solvents (such as DMSO, THF, EtOH, and DCM) and only one absorption band at ~340 nm in H_2O. Their emission wavelengths are at 510–560 nm in organic solvents with weak fluorescence signals, while very slight emission signals were observed in H_2O, which may be ascribed to their good solubility

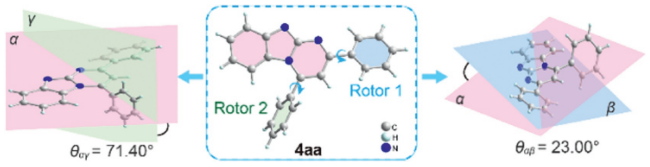

Fig. 3. The crystal structure of **4aa** and its dihedral angles.

in organic solvents while poor solubility in H_2O. For various types of substituents, whether electron-donating/withdrawing groups, aliphatic/aromatic groups, or halogen atoms, their max absorption/emission wavelengths are changed mildly in DMSO (λ_{abs}: 338–356 and 388–410 nm; λ_{em}: 514–553 nm), suggesting slight wavelength-tunable capability of this scaffold, and their absorbance/emission wavelengths would mainly depend on the skeleton of benzo[4,5]imidazo[1,2-*a*]pyrimidine.

The responses for viscosity were examined. As expected, all 15 compounds exhibit fluorescence changes in presence of glycerol (Figs. S2–S4 and Table S2 in Supporting information). Among them, the signal-to-noise ratio (S/N) of **4aa** for viscosity is as high as 102, whereas this parameter for other compounds, for instance, **4p** is as low as 1.3. It follows that the rotors of fluorophore would be a key factor for sensing viscosity. Then the crystal structure of **4aa** was analyzed, as shown in Fig. 3, **4aa** displays three planes in intramolecular. The dihedral angle between benzo[4,5]imidazo[1,2-*a*]pyrimidine (plane α) and rotor 1 (plane β) is $\theta_{\alpha\beta} = 23.00°$, and the dihedral angle between plane α and rotor 2 (plane γ) is $\theta_{\alpha\gamma} = 71.40°$. On one hand, the existing torsion angle would avoid π-π stacking to quench fluorescence. On the other hand, the intramolecular rotations would be restricted as the increase of viscosity, resulting in significant fluorescence enhancement. Owing to high S/N for viscosity, as a proof-of-concept application, we thus selected the compound **4aa** for further investigation.

The selectivity of **4aa** was then explored. Upon addition of common metal ions (Na^+, K^+, Fe^{3+}, Ca^{2+}, Al^{3+}, Cu^{2+}), reactive sulfur species (RSS, including NaHS, Na_2S, Na_2SO_3, $Na_2S_2O_3$, cysteine (Cys), homocysteine (Hcy), glutathione (GSH)), reactive oxygen species (ROS, including H_2O_2 and NaClO), amino acids (lysine (Lys) and arginine (Arg)) and glycerol, **4aa** showed specific respond towards viscosity with remarkable fluorescence enhancement, while other species almost did not cause the fluorescence and absorbance changes (Figs. 4a and b, Fig. S6 in Supporting information). Given that other microenvironments such as polarity may lead to fluorescence variations, the fluorescence spectrum of **4aa** in different solvents were also tested. As shown in Fig. 4c, compared to glycerol (viscosity = 675.09 cp), the effects on different polarity solvents are negligible. These results reveal a good selectivity of **4aa** for viscosity.

To evaluate whether **4aa** can respond to different viscosities, the viscosity values of the different glycerol fractions were measured using a rotational rheometer (at 25 °C). Then the fluorescence spectra of **4aa** at different viscosities were tested, which indicated that the fluorescence emission peak of **4aa** at 490 nm has

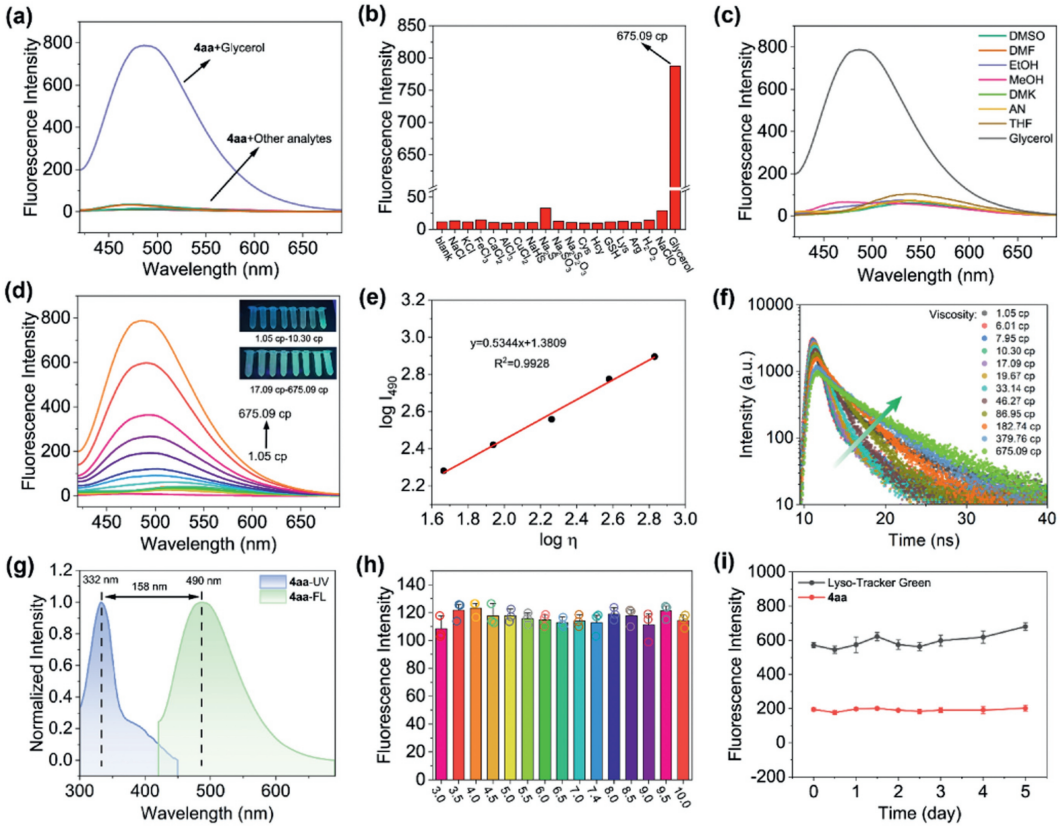

Fig. 4. (a) Fluorescence spectra and (b) Fluorescence intensity of **4aa** in the presence of different analytes, including NaCl, KCl, $FeCl_3$, $CaCl_2$, $AlCl_3$, $CuCl_2$, NaHS, Na_2S, Na_2SO_3, $Na_2S_2O_3$, Cys, Hcy, GSH, Lys, Arg, H_2O_2, NaClO (100 μmol/L, respectively), Glycerol (675.09 cp). (c) Fluorescence spectra of **4aa** in different solvents (DMSO, DMF, EtOH, MeOH, DMK, AN, THF, Glycerol). (d) Fluorescence spectra of **4aa** with different viscosity in the water/glycerol system (1.05–675.09 cp). The inset of (d) shows the corresponding fluorescence observed for **4aa** in different viscosity systems under irradiation at 365 nm UV light. (e) Linear relationship of **4aa** between log I_{490} (I_{490}: fluorescence intensity at 490 nm) and log η (η: viscosity). (f) Fluorescence decay profiles of **4aa** in different viscosities determined with picosecond pulsed excitation at 350 nm (λ_{em} at 490 nm). (g) Normalized fluorescence and ultraviolet absorbance spectra of **4aa** at water/glycerol systems (675.09 cp). (h) Fluorescence intensity of **4aa** in different pH values. (i) Fluorescence spectra of **4aa** compared to the stability of Lyso-Tracker Green. The concentration of **4aa** is 10 μmol/L. All fluorescence spectra were acquired at $\lambda_{ex} = 350$ nm. Data are expressed as the mean ± SD ($n = 3$).

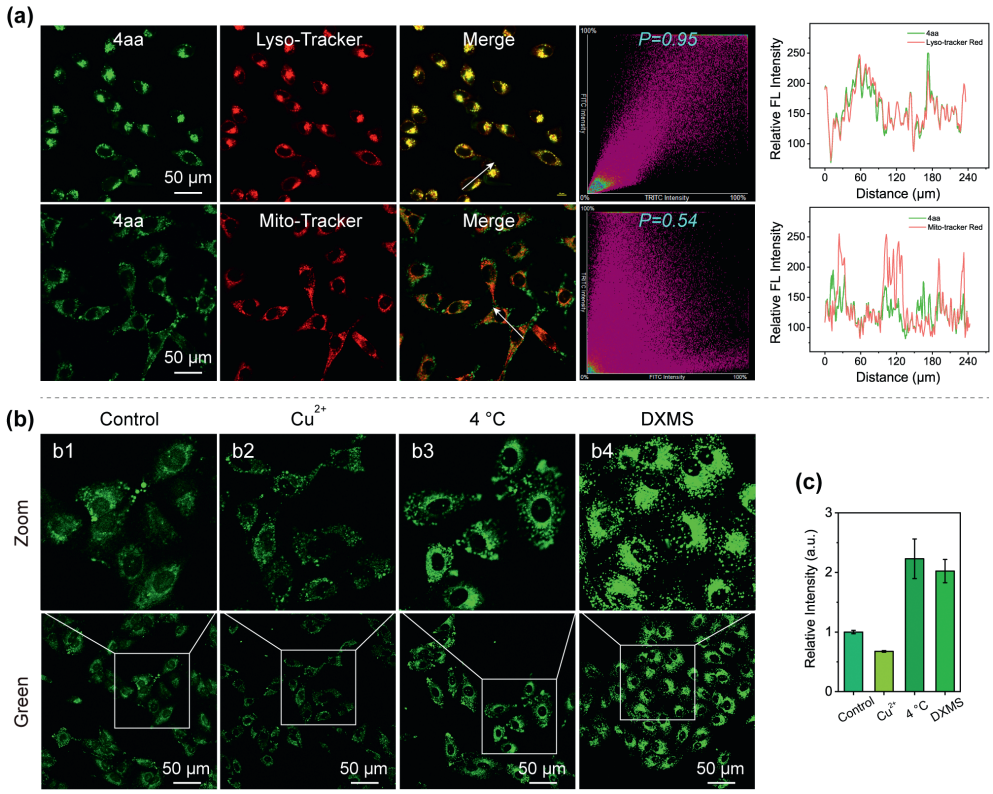

Fig. 5. (a) Fluorescence images of A549 cells co-incubated with **4aa** (10 μmol/L, λ_{ex} = 441 nm) and Lyso-Tracker red (1 μmol/L, λ_{ex} = 561 nm) or Mito-Tracker red (1 μmol/L, λ_{ex} = 561 nm) for 30 min at 37 °C, respectively (Scale bar: 50 μm). (b) Fluorescence images of A549 cells treated with **4aa** (10 μmol/L) only (b1) and pretreated with Cu^{2+} (20 μmol/L, 40 min) (b2) or 4 °C for 30 min (b3) or DXMS (10 μmol/L, 10 min) (b4), respectively, followed by incubation of **4aa** (10 μmol/L). (c) Relative fluorescence intensity of Fig. 5b conducted by Image J. Data are expressed as the mean ± SD (n = 3).

a sharp enhancement as the viscosity value increases from 1.05 cp to 675.09 cp (Fig. 4d), accompanied by the vivid color changes from slight cyan to bright cyan under 365 nm irradiation. Furthermore, a good linear relationship between the fluorescence intensity (log I_{490}) of **4aa** and the viscosity (log η) were recorded based on the Föster-Hoffmann equation (Fig. 4e) [30]. Subsequently, the fluorescence lifetimes were determined at different viscosities, indicating that the fluorescence lifetime of **4aa** increased from 1.73 ns to 5.77 ns with the increase of viscosity from 1.05 cp to 675.09 cp (Fig. 4f). Moreover, the absolute fluorescent quantum yield of **4aa** also increased from 0.3% to 39.9% with the increase of viscosity (Table S4 in Supporting information). In addition, the Stokes shift of **4aa** is as large as 158 nm, which would effectively avoid the interference from excitation light (Fig. 4g). Owing to frequent pH variations in cellular microenvironment, especially in lysosomes, the good pH stability is desired for viscosity-specific fluorescent sensor. To our delight, **4aa** showed excellent pH stability at a wide pH range (pH 3.0–10.0) (Fig. 4h), which is catered to our initial expectation. Moreover, compared to commercial Lyso-Tracker Green, the **4aa** showed a better photostability as depicted in Fig. 4i. Furthermore, when glycerol coexisted with other analytes, **4aa** exhibited a good anti-interference ability, which enables specifically detecting viscosity in complex environments (Figs. S7 and S8 in Supporting information).

Motivated by excellent optical properties in solution, the imaging performance was further evaluated in living cells. First, we assessed the cytotoxicity of **4aa** in A549 cells by using MTT assay and observed over 80% cell viability when the concentration of **4aa** was up to 25 μmol/L (Fig. S9 in Supporting information), suggesting **4aa** has low cytotoxicity. Moreover, the continuous irradiation for 60 min, the fluorescence intensity of **4aa** remained stable in living cells (Fig. S10 in Supporting information), indicating good anti-photobleaching ability of it. Subsequently, colocalization imaging experiments were performed to examine the subcellular targeting capability by co-staining with commercial Lyso-/Mito-Tracker red in A549 cells, respectively. As shown in Fig. 5a, **4aa** can be readily loaded into living cells and displayed a dotted green fluorescence and overlapped very well with the red fluorescence from commercial Lyso-Tracker Red with a high Pearson's coefficient (P = 0.95). However, this parameter of **4aa** with the Mito-Tracker red was only 0.54, manifesting excellent lysosome targeting properties of **4aa**. Moreover, the other 14 compounds were evaluated by colocalization experiments, which also exhibited similar results (Figs. S11–S17 in Supporting information). These results powerfully support our opinions that multiple nitrogen-fused heterocycle benzo[4,5]imidazo[1,2-*a*]pyrimidine skeletons have structural-inherent targeting capability for lysosome.

Inspired by prominent photophysical properties and lysosome-targeting capability, **4aa** was evaluated to monitor the dynamic alterations of lysosomal viscosity. A549 cells were treated with **4aa**, followed by incubation at 37 °C (control) or 4 °C for 30 min, respectively. As depicted in Figs. 5b1 and b3, the cells displayed higher fluorescence intensity at lower incubation temperature (4 °C) than that incubated at 37 °C. Meanwhile, the cells were pretreated with excess heavy metal ions Cu^{2+} (to decrease cell viscosity [31]) showed a reduced fluorescence signal while those pretreated with dexamethasone (DXMS, a kind of glucocorticoid drug, to increase lysosomal viscosity [3]) enhanced significantly (Figs. 5b2, b4). The results elucidated the great potential of **4aa** for mapping dynamic variations of lysosomal viscosity.

As is known, LSD results from defective lysosomal acid hydrolysis enzyme of macromolecules and is characterized by the intralysosomal accumulation of undegraded substrates, increased lysosomal viscosity, and enlarged lysosome volume (Fig. 6a)

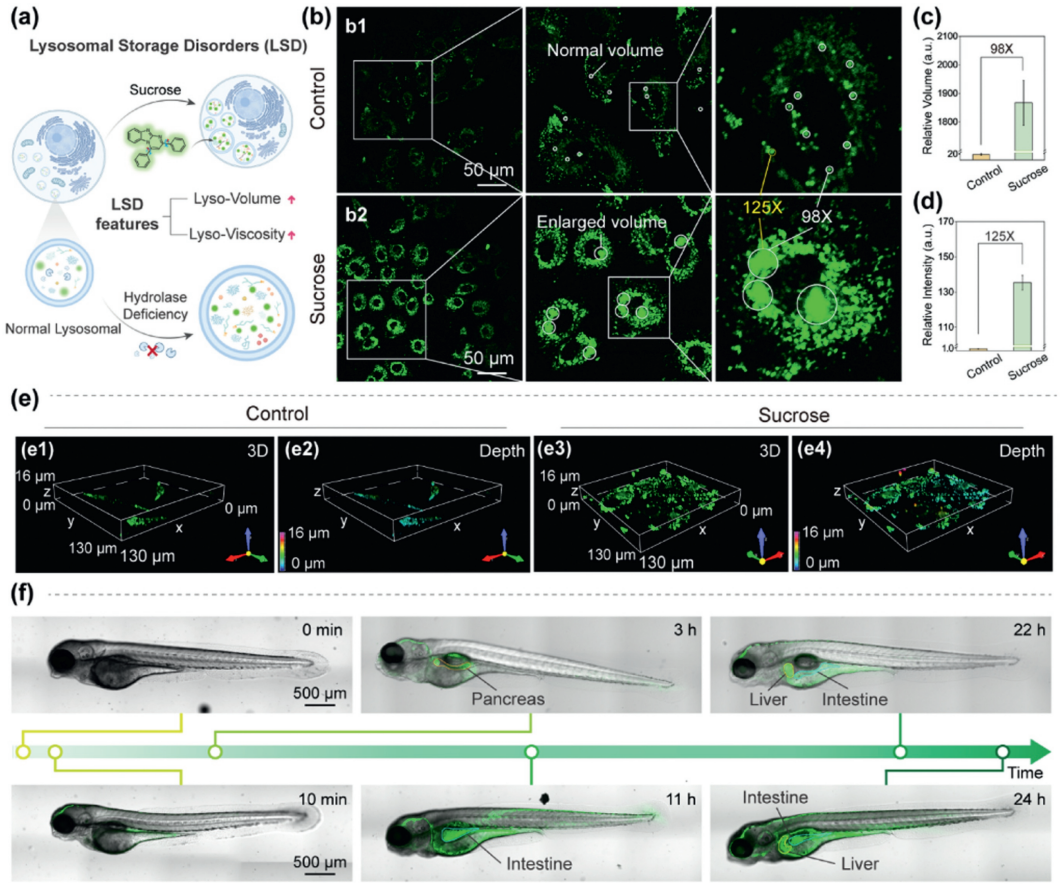

Fig. 6. (a) Schematic representation of characteristics of lysosomal lesions. (b) The changes of lysosomes caused by LSD. (b1) A549 cells are incubated with **4aa** (10 μmol/L, 30 min); (b2) A549 cells pretreated with sucrose (80 mmol/L, 10 min) before incubation **4aa** (10 μmol/L, 30 min), $\lambda_{ex} = 441$ nm. (c, d) Relative lysosomal volume (c) and relative fluorescence intensity (d) of Fig. 6b were analyzed using Image J software. (e) (e1, e3) Z-axis scanning and three-dimensional reconstruction in normal A549 cells (control) and lysosome storage disorders cells (sucrose). (e2, e4) The depth of the cells in e1 and e3. (f) Confocal imaging of zebrafish incubated with **4aa** (10 mmol/L, 0 min, 10 min, 3 h, 11 h, 22 h, 24 h, $\lambda_{ex} = 441$ nm) (Scale bar: 500 μm). Data are expressed as the mean ± SD ($n = 3$).

[32,33]. To observe whether **4aa** could be applied to diagnose LSD, we established the LSD model by pretreating cells with a high concentration of sucrose solution (80 mmol/L) [34-36]. As shown in Figs. 6b–d, after incubation with **4aa**, the experimental group treated with sucrose exhibited a remarkable increase in fluorescence intensity (125-fold) and an enlargement of lysosome volume (98-fold) compared to the control group, demonstrating that not only lysosomal viscosity increases but also lysosome volume enlarges would occur during LSD. Additionally, 3D imaging of lysosomes indicates that the depth of lysosomes in normal cells was approximately 6 μm (Fig. 6e2), whereas the depth of lysosomes in LSD cells increased to approximately 13 μm (Fig. 6e4). The above results manifest the application potential of **4aa** in fluorescence imaging for tracking lysosomal viscosity variations and diagnosing LSD, which may be a promising tool for studying lysosome-related pathology and physiological processes.

Furthermore, the imaging capability of **4aa** was investigated in zebrafish. As shown in Fig. 6f, the dynamic fluorescence signals were observed that transferred from the skin to the pancreas, intestine, and then liver at different times. Such results indicated the metabolic process of **4aa** and displayed an intuitive evaluation of the viscosity of zebrafish organs, which would be useful to monitor the drug-simulated viscosity variations and facilitate new drug discovery.

In summary, a novel and efficient Cu(II)-catalyzed cascade coupling cyclization reaction of aldehyde, 2-aminobenzimidazole, and β-nitroalkenes has been developed for the synthesis of benzo[4,5]imidazo[1,2-*a*]pyrimidine derivatives, and such approach exhibited broad substrate scopes with moderate to good yields. Importantly, this kind of multiple nitrogen-containing fused heterocyclic compound not only demonstrated viscosity-specific fluorescent response with high pH stability but also showed outstanding structural-inherent targeting for lysosome, which displayed excellent capability for detecting lysosomal viscosity and diagnosing LSD in living cells. This work provides an efficient protocol to construct benzo[4,5]imidazo[1,2-*a*]pyrimidine derivatives and an available viscosity-sensitive tool for further exploring lysosome-related physiological and pathological processes, while their absorption and emission wavelength are promised to be extended in future research.

Declaration of competing interest

The authors declare that they have no known competing financial interests or personal relationships that could have appeared to influence the work reported in this paper.

CRediT authorship contribution statement

Jiao Chen: Writing – review & editing, Writing – original draft, Visualization, Validation, Methodology, Investigation, Funding acquisition, Data curation, Conceptualization. **Zihan Zhang:** Writing – original draft, Visualization, Methodology, Investigation, Formal analysis, Data curation. **Guojin Sun:** Software, Investigation, Formal analysis, Data curation. **Yudi Cheng:** Visualization, Validation,

Software, Methodology, Investigation, Funding acquisition, Data curation, Conceptualization. **Aihua Wu:** Methodology, Investigation, Data curation. **Zefan Wang:** Software, Investigation, Formal analysis. **Wenwen Jiang:** Investigation, Data curation. **Fulin Chen:** Writing – review & editing, Supervision, Resources, Methodology, Conceptualization. **Xiuying Xie:** Writing – review & editing, Validation, Resources, Conceptualization. **Jianli Li:** Writing – review & editing, Supervision, Project administration, Funding acquisition, Conceptualization.

Acknowledgments

This work was supported by the National Natural Science Foundation of China (Nos. 22077099, 22171223 and 22307102), the Innovation Capability Support Program of Shaanxi (Nos. 2023-CX-TD-75 and 2022KJXX-32), the Technology Innovation Leading Program of Shaanxi (Nos. 2023KXJ-209 and 2024QCY-KXJ-142), the Key Research and Development Program of Shaanxi (No. 2024GH-ZDXM-22), the Natural Science Basic Research Program of Shaanxi (Nos. 2023-JC-YB-141 and 2022JQ-151), and Young Talent Fund of Association for Science and Technology in Shaanxi, China (No. SWYY202206), the Shaanxi Fundamental Science Research Project for Chemistry & Biology (Nos. 22JHZ010 and 22JHQ080), the Yan'an City Science and Technology Project (No. 2022SLZDCY-002).

Supplementary materials

Supplementary material associated with this article can be found, in the online version, at doi:10.1016/j.cclet.2024.110050.

References

[1] S.R. Bonam, F. Wang, S. Muller, Nat. Rev. Drug Discov. 18 (2019) 923–948.
[2] C. Settembre, R.M. Perera, Nat. Rev. Mol. Cell Biol. 25 (2024) 223–245.
[3] L. Wang, Y. Xiao, W. Tian, L. Deng, J. Am. Chem. Soc. 135 (2013) 2903–2906.
[4] H. Song, W. Zhang, Y. Zhang, et al., Chem. Eng. J. 445 (2022) 136448.
[5] J. Ma, R. Sun, K. Xia, et al., Chem. Rev. 124 (2024) 1738–1861.
[6] D. Su, C.L. Teoh, L. Wang, et al., Chem. Soc. Rev. 46 (2017) 4833–4844.
[7] D. Li, T. Shen, X. Xue, et al., Sci. China Chem. 66 (2023) 2329–2338.
[8] J. Devany, K. Chakraborty, Y. Krishnan, Nano Lett. 18 (2018) 1351–1359.
[9] X. Wang, L. Wang, T. Jin, et al., Sens. Actuators B: Chem. 375 (2023) 132935.
[10] J.J. Chao, H. Zhang, Z.Q. Wang, et al., Anal. Chim. Acta 1285 (2024) 342024.
[11] L. Hu, J. Yang, C. Zhang, et al., Sens. Actuators B: Chem. 398 (2024) 134776.
[12] L. Lian, R. Zhang, S. Guo, et al., Chin. Chem. Lett. 34 (2023) 108516.
[13] L. Zhang, W. Wang, Y.Q. Zhao, et al., Chin. Chem. Lett. (2024), doi:10.1016/j.cclet.2024.109798.
[14] Y.Q. Zhou, Z.Z. Liu, G.M. Qiao, et al., Chin. Chem. Lett. 32 (2021) 3641–3645.
[15] F. Zheng, R. Xiao, S. Huang, et al., Chin. Chem. Lett. (2024), doi:10.1016/j.cclet.2024.109876.
[16] H. Fang, Y. Chen, Z. Jiang, et al., Acc. Chem. Res. 56 (2023) 258–269.
[17] Q. Fu, X. Yang, M. Wang, et al., ACS Nano 18 (2024) 3916–3968.
[18] Y. Yang, M. Ma, L. Shen, et al., Angew. Chem. Int. Ed. 62 (2023) e202310408.
[19] X. Li, J. Wang, F. Huo, C. Yin, Coord. Chem. Rev. 506 (2024) 215713.
[20] Y. Cheng, X. Wang, J. Chen, et al., Chin. Chem. Lett. 35 (2024) 109156.
[21] S.-S. Tseng, J.W. Epstein, H.J. Brabander, G. Francisco, J. Heterocycl. Chem. 24 (1987) 837–843.
[22] R. Alajarin, J.J. Vaquero, J. Alvarez-Builla, et al., Bioorg. Med. Chem. 2 (1994) 323–329.
[23] A.J. Marcus, I. Iezhitsa, R. Agarwal, et al., Eur. J. Pharmacol. Sci. 114 (2018) 245–254.
[24] S.B. Bharate, T.R. Mahajan, Y.R. Gole, et al., Bioorg. Med. Chem. 16 (2008) 7167–7176.
[25] N.A. White, K. Clagg, L.E. Sirois, et al., Org. Lett. 21 (2019) 9527–9531.
[26] M. Rawat, D.S. Rawat, Tetrahedron Lett. 59 (2018) 2341–2346.
[27] J. Wu, H. Luo, T. Wang, et al., Tetrahedron 75 (2019) 1052–1063.
[28] Z. Qin, R. Zhang, S. Ying, Y. Ma, Org. Chem. Front. 9 (2022) 5624–5630.
[29] M. Guo, X. Huang, S. Li, et al., J. Org. Chem. (2023), doi:10.1021/acs.joc.3c01227.
[30] J. Liu, W. Zhang, C. Zhou, et al., J. Am. Chem. Soc. 144 (2022) 13586–13599.
[31] A. Zheng, H. Liu, X. Gao, et al., Anal. Chem. 93 (2021) 9244–9249.
[32] G. Parenti, G. Andria, A. Ballabio, Ann. Rev. Med. 66 (2015) 471–486.
[33] F.M. Platt, A. D'azzo, B.L. Davidson, et al., Nat. Rev. Dis. Primers 4 (2018) 27.
[34] M. Li, J. Fan, H. Li, et al., Biomaterials 164 (2018) 98–105.
[35] I. Hamer, M. Jadot, Exp. Cell Res. 309 (2005) 284–295.
[36] M. Samarani, N. Loberto, G. Soldà, et al., FASEB J. 32 (2018) 5685–5702.